Electrostatic screening of free charge-neutral dipoles/excitons in two-dimensional media

Ke Xiao [1,2,*,†] Chi-Ming Kan [2,3,*] Feng-Ren Fan [4,2] Stuart S. P. Parkin [1] and Xiaodong Cui [2]

[1] *NISE Department, Max Planck Institute of Microstructure Physics, Halle, Germany*

[2] *Physics Department and State Key Laboratory of Optical Quantum Materials, The University of Hong Kong, Pokfulam, Hong Kong, China*

[3] *Department of Chemistry, Hong Kong University of Science and Technology, Clear Water Bay, Hong Kong, China*

[4] *School of Physical Science and Technology, Soochow University, Suzhou 215006, China*

(Received 9 May 2025; revised 27 August 2025; accepted 1 October 2025; published 24 October 2025)

With the shrinking of dimensionality, Coulomb interaction plays a distinct role in two-dimensional (2D) semiconductors owing to the reduced dielectric screening in the out-of-plane direction. Apart from the dielectric screening, free particles such as carriers and dipoles or excitons can also make a non-negligible contribution to the Coulomb interaction. While the Thomas-Fermi model is effective in describing charge carrier screening in three dimensions, the extent of screening resulting from neutral dipoles or excitons in both two and three dimensions remains quantitatively unclear. Here, we present an analytical solution based on linear response theory, offering a comprehensive depiction of the Coulomb screened potential from charge-neutral dipoles or excitons in both 2D and 3D systems, while the free dipole screening effect is much stronger in the 2D case than that in the 3D case. Using the derived screened Coulomb potential, we estimate the exciton binding energy shift arising from the mutual exciton screening effect, which is found to be an order of magnitude larger than that due to exchange-driven exciton-exciton interaction, yielding excellent agreement with the experimental observations. Our work provides a practical and insightful framework for directly analyzing and evaluating Coulomb interaction strength in an excitonic system in atomically thin materials, with implications for the design of electronic and optoelectronic devices.

DOI: 10.1103/9fgx-nq97

I. INTRODUCTION

The emergence of atomically thin two-dimensional (2D) materials not only offers a versatile platform for physical research, but also holds great promise for various applications owing to their intriguing properties. With reduced dimensionality, Coulomb interaction is greatly enhanced due to reduced dielectric screening and spatial confinement [1,2]. This enhanced Coulomb interaction plays a more significant role in the electronic properties of 2D materials than in their three-dimensional (3D) counterparts, usually determining the characteristic optical and electronic properties. Renowned evidence includes the giant exciton binding energy [3–5], significant renormalization of the electronic band gap [6,7], Moiré excitons in 2D heterostructures [8–10], and enhanced superconductivity [11,12]. Achieving an effective modification of the Coulomb interaction is crucial for potential applications based on 2D materials [13–15].

In contrast to the 3D dielectric case, where macroscopic Coulomb screening is well described by a single macroscopic dielectric constant ε_s or, more accurately, a permittivity tensor in the modified Coulomb potential [Fig. 1(a)], macroscopic screening in the 2D dielectric case is highly nonlocal [16–18] and the induced polarization is confined to the 2D plane [Fig. 1(b)], resulting in a suppression of dielectric screening in the out-of-plane direction. The Coulomb potential due to this contrasting dielectric polarization in the 2D case is widely described in the Rytova-Keldysh form [19,20], $V_{2D}(\boldsymbol{\rho}, z) = \frac{e}{8\varepsilon_0 r_0}[H_0(\frac{\varepsilon_s \rho}{r_0}) - Y_0(\frac{\varepsilon_s \rho}{r_0})]$, where H_0 and Y_0 denote Struve and Neumann functions, and $\boldsymbol{\rho}$, r_0, and ε_s are the 2D spatial coordinates, effective screening length, and effective dielectric constant, respectively. It displays logarithmic divergence ($V_{2D}^{\text{app}} = -\frac{e}{4\pi\varepsilon_0 r_0}[\ln(\frac{\varepsilon_s \rho}{2r_0}) + \gamma]$) over a short range and is reduced to the conventional 3D screened potential ($V_{3D} = \frac{e}{4\pi\varepsilon_s\varepsilon_0 r}$) in the long-range limit [Fig. 1(e)].

Apart from screening from the crystal lattice polarization, referred to as dielectric screening, the Coulomb potential can be further screened by free particles, including free charge carriers and charge-neutral dipoles or excitons. Typically, in 3D systems, the screened Coulomb potential arising from charge carriers is well described by the Debye model, Thomas-Fermi model, or Lindhard theory [21]. An exponential damping term is exerted on the long-range Coulomb potential ($V_{3D}^{\text{carrier}} = \frac{e}{4\pi\varepsilon_s\varepsilon_0 r} e^{-r/r_D}$), where r_D is the Debye screening length, making it a short-range potential. For 2D systems, the Coulomb potential can be screened by free carriers through their redistribution as well [Fig. 1(c)]. A quantitative description accounting for the screening effect by free carriers in 2D systems has been developed and discussed in many prior studies

*These authors contributed equally to this work.

†Contact author: ke.xiao@mpi-halle.mpg.de

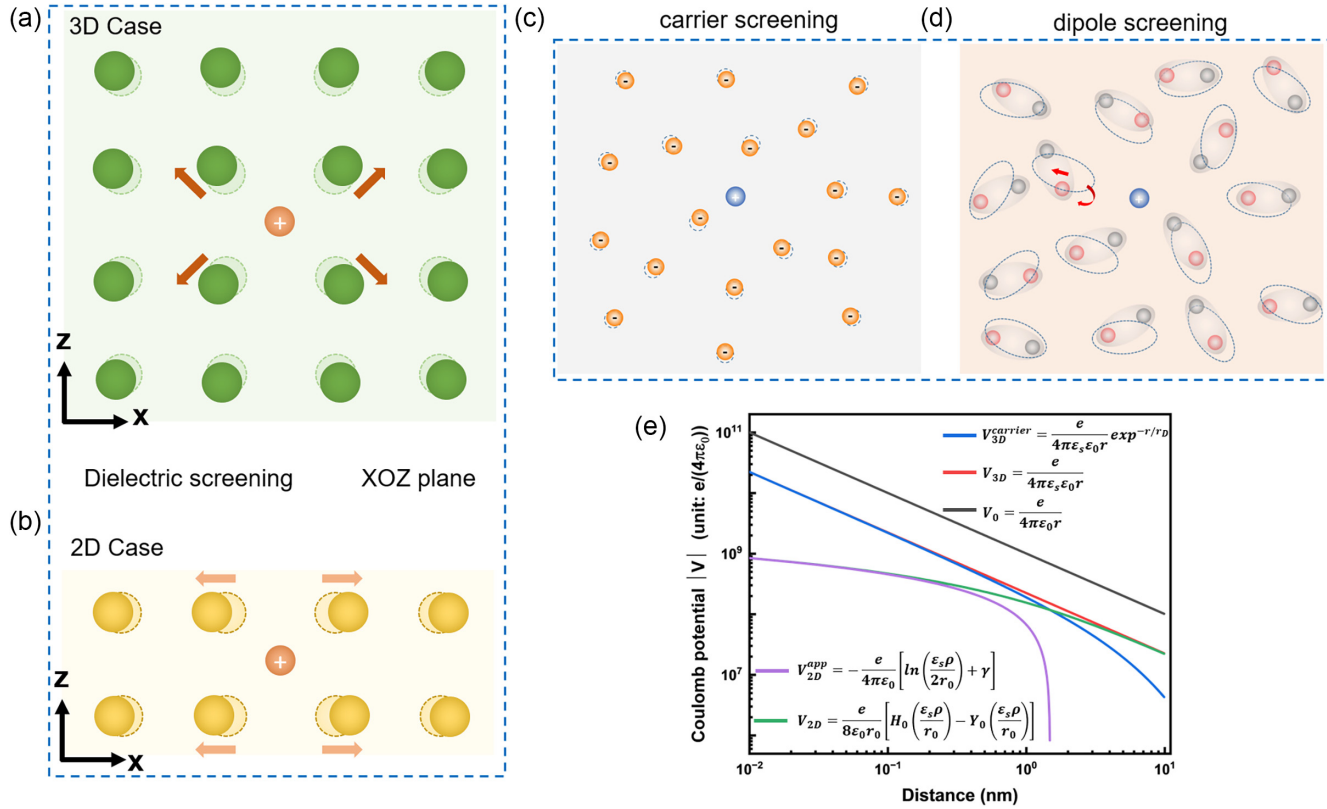

FIG. 1. Schematic illustration of Coulomb screening from dielectric polarization and free particles. Dielectric polarization in the (a) 3D case and (b) 2D case. The dashed spheres indicate the initial position of ions in a crystal lattice, while the solid spheres represent their displaced positions after the introduction of a hypothetical point charge. In the 2D case, the polarization occurs only within the 2D plane, leading to a nonlocal macroscopic screening. (c) Screening by free charge carriers: the dashed circles indicate the initial spatial distribution of carriers and the solid circles show their redistribution following the introduction of a point charge. (d) Screening by free charge-neutral dipoles: the dashed ellipses mark the initial configuration of dipoles, while the solid ellipses show their reoriented and redistributed positions following the introduction of a point charge. (e) Comparison of Coulomb potential under different screening conditions. The gray line shows the bare Coulomb potential in vacuum, $V_0 = \frac{e}{4\pi\varepsilon_0 r}$; the red line shows the Coulomb potential screened by a bulk dielectric, $V_{3D} = \frac{e}{4\pi\varepsilon_s\varepsilon_0 r}$; the blue line includes additional screening by free carriers in a bulk dielectric, $V_{3D}^{\text{carrier}} = \frac{e}{4\pi\varepsilon_s\varepsilon_0 r}e^{-r/r_D}$; the green line represents the Coulomb potential in a 2D lattice, $V_{2D} = \frac{e}{8\varepsilon_0 r_0}[H_0(\frac{\varepsilon_s\rho}{r_0}) - Y_0(\frac{\varepsilon_s\rho}{r_0})]$; and the purple line shows the short-distance approximation of the 2D Coulomb potential, $V_{2D}^{\text{app}} = -\frac{e}{4\pi\varepsilon_0}[\ln(\frac{\varepsilon_s\rho}{2r_0}) + \gamma]$.

[20,22–25]. Notably, Stern derived a 2D screening potential for fermionic carriers in the static limit [22]. However, this approach does not properly account for the dielectric screening of the thin film and surrounding materials, limiting its applicability to layered 2D systems. More recently, Glazov and Chernikov provided an accurate analytical form of the carrier-screened Coulomb potential and demonstrated the breakdown of static carrier screening to estimate the exciton binding energy [25]. On the other hand, free dipoles/excitons can also screen the Coulomb potential via the dipole shift and reorientation [Fig. 1(d)]. One example is small polar molecules in solvents, where dipole screening dominates electrostatic interaction [26–28]. While dipole-induced screening is generally much weaker than carrier-induced screening and often neglected due to the charge neutrality of dipoles/excitons, it can become significant in certain scenarios in the 2D case, particularly at moderate dipole/exciton densities. [29,30] This is because, in 2D systems, dipoles are usually confined to the 2D plane and this orientational constraint leads to the enhanced screening of the Coulomb interaction in plane. As shown in Fig. 1(e), different forms of Coulomb potential are compared, and the screened Coulomb potential from dipoles/excitons remains quantitatively unexplored.

Recently, the screening effect of excitons has been experimentally addressed in an exciton system of monolayer transition metal dichalcogenides (TMDs) [31,32]. However, a general and specific quantitative description and comparison of the screened Coulomb potential arising from charge-neutral dipoles in both the 2D and 3D cases are still lacking. Addressing this gap constitutes the primary focus and key findings of this article.

The outline of the paper is as follows. In Sec. II, we present a detailed derivation of the modified Coulomb potential under a screening effect from charge-neutral dipoles within the framework of linear response theory for both 2D and 3D systems. To validate our approach, we cross verify the results using perturbation theory, as detailed in the Supplemental Material [33]. In Sec. III A, we analyze and compare the screened Coulomb potential from dipole/excitons with the unscreened Coulomb potential in both 2D and 3D systems,

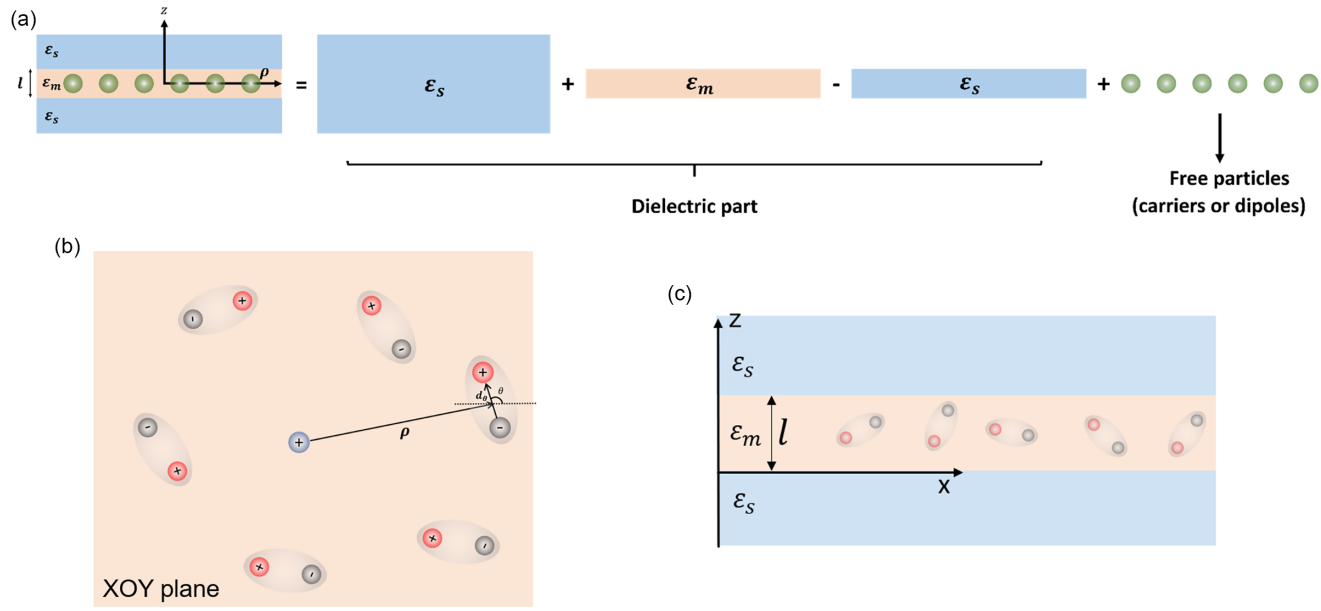

FIG. 2. Schematics of screening effect from charge-neutral dipoles in the 2D case. (a) A dielectric sheet (ε_m) encapsulated in a dielectric environment (ε_s), where the screening effect from the dielectric part and free dipoles are decoupled. (b) Illustration of the charge–dipole interaction in the 2D system. (c) In certain cases, dipoles are sufficiently small and free to rotate in three dimensions, rather than the dipole orientation being strictly confined to the 2D plane.

confirming the enhanced screening effect of free dipoles in the 2D case. In Sec. III B, we apply the derived screened potential to estimate the variation of exciton binding energy with exciton density. The calculated results show good agreement with both theoretical predictions and experimental observations. Overall, our work provides a valuable framework and a convenient tool for analyzing and quantifying the dipole-screened Coulomb interactions in atomically thin materials.

II. DERIVATION OF MODIFIED COULOMB POTENTIAL UNDER SCREENING EFFECT FROM FREE CHARGE-NEUTRAL DIPOLES

A. Preconditions for 2D approximations

Before delving into the detailed derivation of the modified Coulomb potential due to the screening effects of dipoles (excitons) in the 2D case, the impact of thickness of 2D materials on the screening effect should be clarified and the following conditions should be satisfied so that the system can be approximated as a 2D system. We begin with a dielectric sheet (with subscript m) with finite thickness (l) encapsulated in a dielectric environment (with subscript s) [Fig. 2(a)]. There are two key criteria as follows:

(1) $l \ll \lambda_{th}$, where λ_{th} is the thermal de Broglie's wavelength of the electron (typically several to a dozen nm based on different temperature); $l \ll \frac{12\pi^2\hbar^2\varepsilon_s\varepsilon_0}{e^2m}$ (typical several nm, which is slightly smaller than the thermal de Broglie's wavelength), such that the interaction energy remains far below the energy separation between the ground state and the first excited state due to the quantum confinement to avoid the excited state's population [34]. The two conditions on thickness ensure that electron motion perpendicular to the film is exclusively confined to the lowest mode.

(2) $l^2 n \ll 1$, where n is the free particle density, implying that the average relative distance (r_d) between particles is much bigger than the film thickness (l), which means ($l \ll r_d$) [20].

The two criteria allow us to approximate the system as effectively a pure 2D case, ignoring the z dependence along the out-of-plane direction. In other words, under these two conditions, we can confine the dielectric screening of 2D films by introducing 2D polarizability: $\eta^{\text{ind}}(\boldsymbol{r}) = \alpha_{2D}\delta(z)\nabla^2 V(\boldsymbol{\rho}, z=0)$, where $\eta^{\text{ind}}(\boldsymbol{r})$ is the induced bound charge density and $\alpha_{2D} = \varepsilon_0(\varepsilon_m - \varepsilon_s)l$ is the 2D polarizability [2]. Hence, thickness (l) is encoded in α_{2D}, which is not explicitly stated in the Coulomb potential but its effect is implicitly accounted for. Alternatively, one can always start from a finite thickness and apply the procedures of Rytova, Keldysh, and García Flórez *et al.* to calculate the Coulomb potential [19,20,34], where the thickness (l) explicitly appears in the following formula:

$$V^{RK}(\boldsymbol{q}, z_1, z_2) = -\frac{e\cosh\left[q\left(\frac{l}{2}-z_1\right)+\frac{1}{2}\ln\left(\frac{\varepsilon_m+\varepsilon_s}{\varepsilon_m-\varepsilon_s}\right)\right]\cosh\left[q\left(\frac{l}{2}+z_2\right)+\frac{1}{2}\ln\left(\frac{\varepsilon_m+\varepsilon_s}{\varepsilon_m-\varepsilon_s}\right)\right]}{q\varepsilon_m\varepsilon_0\sinh\left[ql+\ln\left(\frac{\varepsilon_m+\varepsilon_s}{\varepsilon_m-\varepsilon_s}\right)\right]}, \quad (1)$$

where $|z_1|,\ |z_2| \leqslant \frac{l}{2}$ correspond to the position of the two charges along the out-of-plane direction. By taking the aforementioned two criteria, the z dependence is eliminated and the simplified potential has the form $V^{RK}(\boldsymbol{q}, z_1, z_2) \approx V^{RK}_{\text{app}}(\boldsymbol{q}) = \frac{e}{\varepsilon_0 q(2\varepsilon_s+\varepsilon_m l q)}$. Under this approximation, modeling both the source and test charges using the ground-state wave function of the 1D infinite well ($u_1(z)$) yields the same Coulomb potential as treating them as rigid pointlike objects,

$$V^{RK}_{qc}(\boldsymbol{q}) = \int_{-\frac{l}{2}}^{\frac{l}{2}}\int_{-\frac{l}{2}}^{\frac{l}{2}} dz_1 dz_2 u_1^2(z_1)u_1^2(z_2)V^{RK}(\boldsymbol{q}, z_1, z_2) \approx V^{RK}_{\text{app}}(\boldsymbol{q}). \tag{2}$$

It should be noted that the quantum confinement effect, which is particularly significant in the 2D case, is already incorporated through the approximation of strict 2D under the given preconditions.

Thus, these two approaches, i.e., starting directly with a 2D film of negligible thickness or approximating after accounting for finite thickness, are equivalent. For simplicity, we adopt the first approach in the following derivations, treating the dielectric sheet as infinitely thin and confining free dipoles to the 2D plane.

B. Calculation of induced charge density associated with the dipoles based on linear response theory

Unlike charge carriers, electric dipoles ($\boldsymbol{p} = e\boldsymbol{d}$) are charge neutral as a whole, but possess a finite charge-separated vector. To incorporate the effect of dipole screening in the 2D case, we start with a system in thermodynamic equilibrium with a uniform dipole density ($n_{\text{dipole}}(\boldsymbol{\rho}) = \text{cons.}$) as the Jellium model [35]. The system is perturbed by introducing a point charge ($e\delta(\boldsymbol{r})$) at the origin and at time t_0, described by a time-dependent perturbative term ($H_{1,s}(t) = \{^{0,\ t \leqslant t_0}_{U_I(t),\ t > t_0}$).

Under the interaction picture and within the framework of linear response theory, the change in the expectation value of an operator is given by $\langle \hat{O}^{\text{ind}}(t)\rangle = -i\hbar^{-1}\int_{t_0}^{t} dt' \langle[\hat{O}_I(t), U_I(t)]\rangle$. For the dipolar density $[\hat{\boldsymbol{P}}(\boldsymbol{\rho}, t)]$, which couples to the gradient of the Coulomb potential from the point charge (∇V^{ext}), the induced dipolar density can be expressed as

$$\left\langle \hat{\boldsymbol{P}}_i^{\text{ind}}(\boldsymbol{\rho},\ t)\right\rangle = -i\hbar^{-1}\int_{t_0}^{t} dt' \iint d\boldsymbol{\rho}' \chi_{\boldsymbol{P},ij}(\boldsymbol{\rho},\ \boldsymbol{\rho}';t,t')[\nabla V^{\text{ext}}(\boldsymbol{\rho}',\ t')]_j, \tag{3}$$

where $\chi_{\boldsymbol{P},ij}(\boldsymbol{\rho},\ \boldsymbol{\rho}';t,t') = -i\hbar^{-1}\Theta(t-t')\langle[\hat{\boldsymbol{P}}_i(\boldsymbol{\rho},\ t), \hat{\boldsymbol{P}}_j(\boldsymbol{\rho}',\ t')]\rangle$ is the tensorial dipolar density–dipolar density response function. Here, $\hat{\boldsymbol{P}}_i(\boldsymbol{\rho}, t)$ represents the dipolar density's component along the i-th direction at position $\boldsymbol{\rho}$ and time t and $\Theta(t) = -\lim_{\eta\to 0^+}\frac{1}{2\pi i}\int_{-\infty}^{\infty} d\omega \frac{e^{-i\omega t}}{\omega+i\eta}$ is the Heaviside step function. This tensorial response function is mathematically cumbersome, particularly because the external electric field $\boldsymbol{E} = -\nabla V^{\text{ext}}(\boldsymbol{\rho}',\ t')$ is spatially nonuniform. To simplify the calculation of the potential energy $U_I(t)$ coupled to dipolar density $\hat{\boldsymbol{P}}(\boldsymbol{\rho}, t)$, we start from the classical picture of a dipole consisting of two opposite charges separated by a vector $\boldsymbol{d}_\theta$. We decomposed the dipolar density into discrete orientation subcomponents $\boldsymbol{P}_{\theta_j}(\boldsymbol{\rho},\ t)$ along orientations θ_j ($\theta_j = \frac{2\pi j}{N},\ j = 1, 2, \ldots, N$): $\boldsymbol{P}(\boldsymbol{\rho},\ t) = \sum_{j=1}^{N}\boldsymbol{P}_{\theta_j}(\boldsymbol{\rho},\ t) = \sum_{j=1}^{N} n_{\theta_j}(\boldsymbol{\rho},\ t)e\boldsymbol{d}_{\theta_j}$, where $n_{\theta_j}(\boldsymbol{\rho}, t)$ is the dipole density for the dipoles aligned along θ_j. The interaction energy is then $U_I(t) = \sum_{j=1}^{N}\hat{\boldsymbol{P}}_{\theta_j}(\boldsymbol{\rho}, t)\cdot[\nabla V^{\text{ext}}(\boldsymbol{\rho},\ t)] = \sum_{j=1}^{N}\hat{n}_{\theta_j}(\boldsymbol{\rho}, t)e[V^{\text{ext}}(\boldsymbol{\rho}+\frac{\boldsymbol{d}_{\theta_j}}{2}, t) - V^{\text{ext}}(\boldsymbol{\rho}-\frac{\boldsymbol{d}_{\theta_j}}{2}, t)]$. This leads to the induced dipolar density,

$$\langle\hat{\boldsymbol{P}}^{\text{ind}}(\boldsymbol{\rho}, t)\rangle = -i\hbar^{-1}e\int_{t_0}^{t} dt' \iint d\boldsymbol{\rho}' \sum_{j=1}^{N}\sum_{f=1}^{N}\boldsymbol{d}_{\theta_f} \times\left\langle\left[\hat{n}_{\theta_f}(\boldsymbol{\rho}, t), \hat{n}_{\theta_j}(\boldsymbol{\rho}', t')\right]\right\rangle e \times\left[V^{\text{ext}}\left(\boldsymbol{\rho}'+\frac{\boldsymbol{d}_{\theta_j}}{2}, t'\right) - V^{\text{ext}}\left(\boldsymbol{\rho}'-\frac{\boldsymbol{d}_{\theta_j}}{2}, t'\right)\right]. \tag{4}$$

Note that $\hat{n}_{\theta_f}(\boldsymbol{\rho}, t) = g(\theta_j)\hat{n}_{\text{dipole}}(\boldsymbol{\rho}, t)\Delta\theta$, where $g(\theta_j)$ is the angular distribution function and $\Delta\theta = \frac{2\pi}{N}$. In a 2D exciton/dipole system, one typically considers an isotropic and highly randomized in-plane dipole distribution, such that the angular distribution function $g(\theta) \approx \text{cons.}$. Moreover, $\langle[\hat{n}_{\theta_f}(\boldsymbol{\rho}, t), \hat{n}_{\theta_j}(\boldsymbol{\rho}', t')]\rangle \propto \delta_{fj}$ since the dipoles with different orientation are uncorrelated. This implies that the dipole density along θ_f couples only to its own potential energy contribution $\hat{\boldsymbol{P}}_{\theta_f}(\boldsymbol{\rho}, t)\cdot[\nabla V^{\text{ext}}(\boldsymbol{\rho},\ t)]$. Thus, Eq. (4) reduces to

$$\langle\hat{\boldsymbol{P}}^{\text{ind}}(\boldsymbol{\rho}, t)\rangle = -i\hbar^{-1}e^2\sum_{j=1}^{N}\boldsymbol{d}_{\theta_j}\int_{t_0}^{t} dt' \iint d\boldsymbol{\rho}' g(\theta_j)\Delta\theta \times\langle[\hat{n}_{\text{dipole}}(\boldsymbol{\rho}, t), \hat{n}_{\text{dipole}}(\boldsymbol{\rho}', t')]\rangle \times\left[V^{\text{ext}}\left(\boldsymbol{\rho}'+\frac{\boldsymbol{d}_{\theta_j}}{2}, t'\right) - V^{\text{ext}}\left(\boldsymbol{\rho}'-\frac{\boldsymbol{d}_{\theta_j}}{2}, t'\right)\right]. \tag{5}$$

Compared with the definition of dipolar density, $\langle\hat{\boldsymbol{P}}^{\text{ind}}(\boldsymbol{\rho}, t)\rangle = \sum_{j=1}^{N}\boldsymbol{d}_{\theta_j}e\langle\hat{n}_{\theta_j}(\boldsymbol{\rho}, t)\rangle$, we obtain

$$\langle\hat{n}_{\theta_j}(\boldsymbol{\rho},\ t)\rangle = g(\theta_j)\Delta\theta\int_{-\infty}^{+\infty} dt' \iint d\boldsymbol{\rho}' \chi_{\text{dipole}} \times(\boldsymbol{\rho}, \boldsymbol{\rho}';t,\ t')eV(\boldsymbol{\rho}', \boldsymbol{d}_{\theta_j},\ t'), \tag{6}$$

where $\chi_{\text{dipole}}(\boldsymbol{\rho}, \boldsymbol{\rho}';t,t') = -\frac{i}{\hbar}\Theta(t-t')\langle[\hat{n}_{\text{dipole}}(\boldsymbol{\rho}, t), \hat{n}_{\text{dipole}}(\boldsymbol{\rho}', t')]\rangle$ is the density-density correlation function and $eV(\boldsymbol{\rho}', \boldsymbol{d}_{\theta_j}, t') = [eV^{\text{ext}}(\boldsymbol{\rho}'+\frac{\boldsymbol{d}_{\theta_j}}{2}, t') - eV^{\text{ext}}(\boldsymbol{\rho}'-\frac{\boldsymbol{d}_{\theta_j}}{2}, t')]$ is the effective potential energy. Thus, although we started from a vectorial quantity, in the specific case of an isotropic and uncorrelated dipole distribution subject to an isotropic perturbation from a point charge, which also does not have any direction preference, the full tensorial response simplifies in terms of solving the scalar response function.

For a translationally invariant system and time-independent perturbation, the dipole density-density response function depends only on relative coordinates and time differences: $\chi_{\text{dipole}}(\boldsymbol{\rho}, \boldsymbol{\rho}';t,t') = \chi_{\text{dipole}}(\boldsymbol{\rho}-\boldsymbol{\rho}';t-t')$. In the static limit ($\omega \to 0$), the Fourier transformation (FT) of the induced dipole density can be

expressed as $\langle \hat{n}_{\theta_j}(\boldsymbol{q})\rangle = g(\theta_j)\Delta\theta\,\chi_{\text{dipole}}(\boldsymbol{q})eV(\boldsymbol{q}) = g(\theta_j)\Delta\theta\,\chi_{\text{dipole}}(\boldsymbol{q})e(2iV^{\text{ext}}(\boldsymbol{q})\sin(\boldsymbol{q}\cdot\frac{\boldsymbol{d}_{\theta_j}}{2}))$, where $\chi_{\text{dipole}}(\boldsymbol{q}) = \frac{1}{S}\sum_{\boldsymbol{k}}\frac{f(\epsilon_{k+q})-f(\epsilon_k)}{\epsilon_{k+q}-\epsilon_k}$ [21,36]; $f(\epsilon_k)$ represents the Bose-Einstein statistic due to dipoles being bosonic entities and S is the real space area of the 2D system.

The corresponding induced charge density associated with the dipoles is

$$\langle \eta^{\text{ind}}_{\text{dipole}}(\boldsymbol{\rho}, z=0)\rangle = e\sum_{j=1}^{N}\left[n^{\text{ind}}_{\theta_j}\left(\boldsymbol{\rho}-\frac{\boldsymbol{d}_{\theta_j}}{2}, z=0\right) - n^{\text{ind}}_{\theta_j}\left(\boldsymbol{\rho}+\frac{\boldsymbol{d}_{\theta_j}}{2}, z=0\right)\right]. \tag{7}$$

FT yields

$$\eta^{\text{ind}}_{\text{dipole}}(\boldsymbol{q}, z=0) = e^2\chi_{\text{dipole}}(\boldsymbol{q})V(\boldsymbol{q})\sum_{j=1}^{N}4g(\theta_j)\Delta\theta\sin^2\left(\boldsymbol{q}\cdot\frac{\boldsymbol{d}_{\theta_j}}{2}\right). \tag{8}$$

Alternatively, one can also start from the $\langle\eta^{\text{ind}}_{\text{dipole}}(\boldsymbol{\rho})\rangle = -\nabla\cdot\langle \boldsymbol{P}^{\text{ind}}(\boldsymbol{\rho})\rangle$ to calculate the charge density associated with the dipoles based on Eq. (5). We obtain $\langle\eta^{\text{ind}}_{\text{dipole}}(\boldsymbol{q})\rangle = i\sum_{j=1}^{N}(\boldsymbol{q}\cdot\boldsymbol{d}_{\theta_j})e\langle n^{\text{ind}}_{\theta_j}(\boldsymbol{q})\rangle \approx e^2\chi_{\text{dipole}}(\boldsymbol{q})V(\boldsymbol{q})\sum_{j=1}^{N}4g(\theta_j)\Delta\theta\sin^2(\boldsymbol{q}\cdot\frac{\boldsymbol{d}_{\theta_j}}{2})$, which is identical to Eq. (8).

Since the isotropic and a highly randomized dipole system ($g(\theta)\approx\frac{1}{2\pi}$) are considered and the dipole orientation is confined in the 2D plane in a semiclassical way, $\sum_{j=1}^{N}4g(\theta_j)\Delta\theta\sin^2(\boldsymbol{q}\cdot\frac{\boldsymbol{d}_{\theta_j}}{2}) \approx \frac{1}{\pi}\int_0^{2\pi}d\theta\{1-\cos[qd\cos(\theta)]\} = 2[1-J_0(qd)]$, where J_0 is the zeroth-order Bessel function. The induced charge density can be further simplified as

$$\eta^{\text{ind}}_{\text{dipole}}(\boldsymbol{q}, z=0) = 2e^2\chi_{\text{dipole}}(\boldsymbol{q})V^{\text{ext}}(\boldsymbol{q})[1-J_0(qd)]. \tag{9}$$

We cross checked the induced charge density associated with dipoles by perturbation theory to calculate the charge density associated with dipoles, which yields the same results as Eq. (8). (More details are given in the Supplemental Material [33].)

C. Screened Coulomb potential from free dipoles

1. 2D dipoles in 2D plane

After the calculation of the induced charge density, we return to the Poisson's equation, and the screened Coulomb potential [$V(\boldsymbol{r})$] arising from the external point charge at the origin can be expressed as

$$\nabla^2V(\boldsymbol{r}) = \underbrace{-\frac{e}{\varepsilon_0}\delta(\boldsymbol{r})}_{\text{point charge}} \underbrace{-\frac{1}{\varepsilon_0}\alpha_s\nabla^2V(\boldsymbol{r})}_{3D\text{ dielectric}} \underbrace{-\frac{1}{\varepsilon_0}(\alpha_m^{2D}-\alpha_s^{2D})\nabla_\rho^2V(\boldsymbol{\rho}, z=0)\delta(z)}_{2D\text{ dielectric}} \underbrace{-\frac{1}{\varepsilon_0}\eta^{\text{ind}}_{\text{dipole}}(\boldsymbol{\rho}, z=0)\delta(z)}_{\text{free dipole screening}}. \tag{10}$$

As illustrated in Fig. 2(a), ε_0 denotes vacuum permittivity, the first term corresponds to the point charge, the next two terms describe the contribution from dielectric surroundings, including the 3D surrounding part ($\frac{1}{\varepsilon_0}\alpha_s\nabla^2V(\boldsymbol{r})$) and bound charges in the 2D plane ($\frac{1}{\varepsilon_0}(\alpha_m^{2D}-\alpha_s^{2D})\nabla_\rho^2V(\boldsymbol{\rho}, z=0)\delta(z)$), α_s is the 3D polarizability, and α_s^{2D} and α_m^{2D} represent the 2D polarizabilities of the surroundings and dielectric sheet, which are linked to the macroscopic polarization by $\boldsymbol{P}_s = -\alpha_s\nabla V(\boldsymbol{r})$, $\boldsymbol{P}_s^{2D} = -\alpha_s^{2D}\nabla_\rho V(\boldsymbol{\rho}, z=0)$, and $\boldsymbol{P}_m^{2D} = -\alpha_m^{2D}\nabla_\rho V(\boldsymbol{\rho}, z=0)$, respectively. The last term encodes the screening effect from free dipoles. As discussed in Sec. II A, we treat the 2D film as having negligible thickness and confine the induced dipolar charge density to the XOY plane by introducing 3D induced charge density $\eta^{\text{ind}}_{\text{dipole}}(\boldsymbol{r}) = \eta^{\text{ind}}_{\text{dipole}}(\boldsymbol{\rho}, z=0)\delta(z)$.

Then, performing an FT on both sides in the static limit ($\omega\to 0$), we obtain

$$(q^2+k_z^2)V(\boldsymbol{q}, k_z) = -\frac{1}{\varepsilon_s\varepsilon_0}\left[e + q^2\frac{\alpha_{2D}}{2\pi}\int_{-\infty}^{\infty}V(\boldsymbol{q}, k_z)dk_z\right] - \frac{e^2}{\pi\varepsilon_s\varepsilon_0}\chi_{\text{dipole}}(\boldsymbol{q})[1-J_0(qd)] \times\int_{-\infty}^{\infty}V(\boldsymbol{q}, k_z)dk_z, \tag{11}$$

where $\varepsilon_s\varepsilon_0 = \varepsilon_0+\alpha_s$, $\alpha_{2D} = \alpha_m^{2D}-\alpha_s^{2D}$.

Taking the derivative of both sides with respect to k_z yields

$$(q^2+k_z^2)\frac{dV(\boldsymbol{q}, k_z)}{dk_z} + 2k_zV(\boldsymbol{q}, k_z) = 0, \tag{12}$$

whose general solution is $V(\boldsymbol{q}, k_z) = (\frac{C}{q^2+k_z^2})$ and $V(\boldsymbol{q}, z=0) = \frac{1}{2\pi}\int V(\boldsymbol{q}, k_z)dk_z = \frac{C}{2q}$. Substituting $V(\boldsymbol{q}, z=0)$ in Eq. (11) allows us to determine the coefficient C, giving the screened Coulomb potential due to free dipoles in reciprocal space,

$$V_{2D}^{2D\text{ dipole}}(\boldsymbol{q},\ z=0) = \frac{e}{q(2\varepsilon_s\varepsilon_0+q\alpha_{2D}) - 2e^2\chi_{\text{dipole}}(\boldsymbol{q})[1-J_0(qd)]}. \tag{13}$$

We note that one can, in principle, iteratively calculate the modified Coulomb potential through Poisson's equation [Eq. (11)], and induced charge density through linear response theory until the modified Coulomb potential converges, as shown in Fig. S1(a) in the Supplemental Material [33]. Alternatively, many earlier works [2,22,25] adopt the more direct approach of solving the self-consistent Poisson's equation, as depicted schematically in Fig. S1(b) in the Supplemental Material [33], thereby avoiding complex iterative calculations. Here, we follow the latter approach to directly solve the self-consistent Poisson's equation and obtain a closed-form analytical expression for the screened Coulomb potential.

TABLE I. Coulomb potential in 2D and 3D systems without screening, and with carrier screening and dipole screening, respectively.

	2D	3D
Dielectric screening only	$\frac{e}{q(2\varepsilon_s\varepsilon_0+\alpha_{2D}q)}$ [a]	$\frac{e}{(\varepsilon_m\varepsilon_0 q^2)}$
Carrier screening	$\frac{e}{q(2\varepsilon_s\varepsilon_0+q\alpha_{2D})-e^2\chi_{\text{carrier}}(\boldsymbol{q})}$ [b]	$\frac{e}{\varepsilon_m\varepsilon_0 q^2-e^2\chi_{\text{carrier}}(\boldsymbol{q})}$ [c]
Dipole screening	2D dipole: $\frac{e}{q(2\varepsilon_s\varepsilon_0+q\alpha_{2D})-2e^2\chi_{\text{dipole}}(\boldsymbol{q})[1-J_0(qd)]}$	$\frac{e}{\varepsilon_m\varepsilon_0 q^2-2e^2\chi_{\text{dipole}}(\boldsymbol{q})(1-j_0(qd))}$ [d]
	3D dipole: $\frac{e}{q(2\varepsilon_s\varepsilon_0+q\alpha_{2D})-2e^2\chi_{\text{dipole}}(\boldsymbol{q})(1-j_0(qd))}$	

[a]Reference [2].
[b]References [20,25].
[c]Lindhard function.
[d]The long wavelength approximation ($q \to 0$) result was discussed in Ref. [37].

2. 3D dipoles in 2D plane

Beyond the case of dipoles restricted to in-plane motion and orientation, we extend our analysis to a more general scenario where dipoles are free to rotate in 3D space but remain confined spatially to the 2D plane, referred to as a 3D dipole in a 2D plane [Fig. 2(c)]. This extension is motivated by practical situations, such as electrolyte molecules in three-dimensional space near a two-dimensional film, as discussed in Refs. [26–28]. For such 3D dipoles, the orientation θ_j corresponds to solid angle (θ_{j_1}, ϕ_j), with $\theta_{j_1} = \frac{\pi j_1}{N_1}$ and $\phi_{j_2} = \frac{2\pi j_2}{N_2}$, and the induced dipole density runs over all orientations, $\eta^{\text{ind}}_{\text{dipole}}(\boldsymbol{q}, z) = \sum_{j_1=1}^{N_1}\sum_{j_2=2}^{N_2}\sin\theta_{j_1}\Delta\theta\Delta\phi\eta^{\text{ind}}_{(\theta_{j_1},\phi_{j_2})} \approx \frac{1}{4\pi}\int_0^{2\pi} d\phi \int_0^{\pi}\sin\theta d\theta \eta^{\text{ind}}_{(\theta_{j_1},\phi_{j_2})}$. Following Rytova and Keldysh's treatment for a 2D film of finite thickness to solve Poisson's equation, the induced charge density associated with dipoles is calculated and can be effectively expressed as $\eta^{\text{ind}}_{\text{dipole}}(\boldsymbol{q}) = 2e^2\chi_{\text{dipole}}(\boldsymbol{q})[1 - j_0(qd)]V(\boldsymbol{q})$, where j_0 is the zeroth-order spherical Bessel function and the corresponding approximated 2D screened Coulomb potential by 3D dipoles is given by

$$V_{2D}^{3D\ \text{dipole}}(\boldsymbol{q}) = \frac{e}{q(2\varepsilon_s\varepsilon_0 + \alpha_{2D}q) - 2e^2\chi_{\text{dipole}}(\boldsymbol{q})[1 - j_0(qd)]}. \quad (14)$$

The derivation follows a similar procedure outlined in previous sections, with full details provided in the Supplemental Material [33]. The resulting expression is structurally similar to Eq. (13). The key difference is the function $j_0(qd)$, which accounts for dipole orientation in 3D space, replacing $J_0(qd)$, which describes dipole orientation confined to the 2D plane.

3. Dipoles in 3D case

Finally, for dipoles in a fully 3D system, we use the same strategy as for free carriers in 3D, where the screened potential is obtained using conventional Lindhard theory (see the Supplemental Material [33] and Refs. [21,36]). By analogy, the screened potential in the 3D system arising from free dipoles is

$$V_{3D}^{\text{dipole}}(\boldsymbol{q}) = \frac{e}{\varepsilon_m\varepsilon_0 q^2 - 2e^2\chi_{\text{dipole}}(\boldsymbol{q})[1 - j_0(qd)]}. \quad (15)$$

For comparison, Table I summarizes the Coulomb potential under different screening conditions: dielectric screening only, carrier screening, and dipole screening in both 2D and 3D. Among these screened Coulomb potentials, the dielectric screening in both 2D and 3D is well established: In the 3D case, the Coulomb potential in momentum space is $V^{3D}(\boldsymbol{q}) = \frac{e}{\varepsilon_m\varepsilon_0 q^2}$ and in real space is $V^{3D}(\boldsymbol{r}) = \frac{e}{4\pi\varepsilon_m\varepsilon_0 r}$. In the 2D case, the corresponding Coulomb potentials in momentum space and real space are $V^{2D}(\boldsymbol{q}) = \frac{e}{q(2\varepsilon_s\varepsilon_m+\alpha_{2D}q)}$ and $V^{2D}(\boldsymbol{\rho}) = \frac{e}{8\varepsilon_0 r_0}[H_0(\frac{\varepsilon_s\rho}{r_0}) - Y_0(\frac{\varepsilon_s\rho}{r_0})]$, respectively. We compared these dielectric screened Coulomb potentials in real space in Fig. 1(e).

As for the carrier screening effect, in the 3D case, the screened Coulomb potential from free carriers is $V^{3D}_{\text{carrier}}(\boldsymbol{q}) = \frac{e}{\varepsilon_m\varepsilon_0 q^2 - e^2\chi_{\text{carrier}}(\boldsymbol{q})}$ in momentum space, reducing to Yukawa potential $V^{3D}(\boldsymbol{r}) = \frac{e}{4\pi\varepsilon_m\varepsilon_0 r}e^{-\kappa r}$ in real space in the long-wavelength limit ($q \to 0$), where $\kappa = \sqrt{\frac{e^2}{\varepsilon_m\varepsilon_0}\frac{\partial n_{\text{carrier}}}{\partial\mu}}$ and μ is the chemical potential, with the analogous 2D expression obtained from the Lindhard function, $V^{2D}(\boldsymbol{q}) = \frac{e}{q(2\varepsilon_s\varepsilon_m+\alpha_{2D}q)-e^2\chi_{\text{carrier}}(\boldsymbol{q})}$ [25].

As shown in the previous section, we provide analytical expressions for the screened Coulomb potential arising from free dipoles in both 3D and 2D cases, although eariler work [37] has discussed dipole screening only under the long-wavelength approximation in the 3D case. It should be noted that in the free-particle screened Coulomb potential, the forms of $\chi_{\text{carrier}}(\boldsymbol{q})$ and $\chi_{\text{dipole}}(\boldsymbol{q})$ indicate that the Coulomb potential remains radially symmetric because homogeneous particles, whether charge carriers or charge-neutral dipoles, do not break the in-plane rotational symmetry.

III. DISCUSSION OF THE SCREENED COULOMB POTENTIAL

A. Enhanced free dipole screening effect in 2D case

To investigate the screening effect induced by free dipoles, we calculate and plot the screened Coulomb potential using our derived formalism (Table I), as shown in Fig. 3. The dipole-screened Coulomb potential depends on both the doping density (n_{dipole}) and dipole size (d). For illustrative purposes and as a practical example to evaluate the modified Coulomb potential, we set $d = 1.3$ nm, which is the typical exciton Bohr radius in monolayer TMDs [38] and $n_{\text{dipole}} = 10^{11}$ cm^{-2} in a 2D system. For comparison, the dipole density in a 3D system is chosen as $n_{\text{dipole}} = (10^{11})^{\frac{3}{2}}$ cm^{-3}, ensuring a consistent reference between 2D and 3D systems. Figure 3(a) shows the momentum-space Coulomb potential

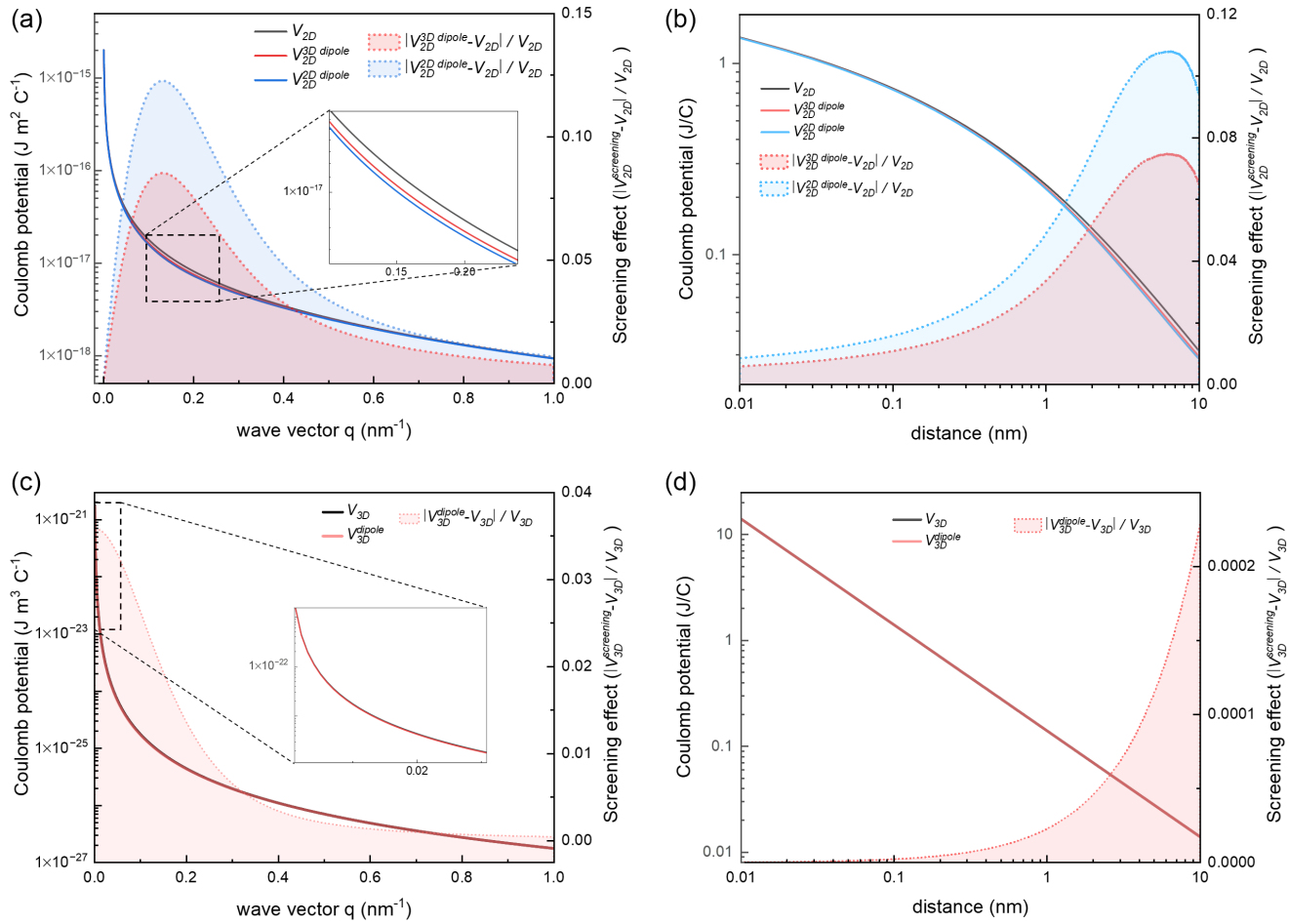

FIG. 3. Screened Coulomb potential from free dipoles in momentum and real space. (a), (b) Comparison of the bare 2D Coulomb potential (V_{2D}) (black solid line), 2D screened Coulomb potential in the presence of 3D dipoles ($V_{2D}^{3D\ \mathrm{dipole}}$) (red solid line), and 2D dipoles ($V_{2D}^{2D\ \mathrm{dipole}}$) (blue solid line) in (a) momentum space and (b) real space. The corresponding relative screening effect, $\frac{|V_{2D}^{\mathrm{screening}}-V_{2D}|}{V_{2D}}$, is indicated by dashed lines and shaded areas. The dipole size and dipole density are set to $d = 1.3$ nm and $n_{\mathrm{dipole}} = 10^{11}$ cm^{-2}, respectively. The inset in (a) shows a zoom-in view of the dashed region in (a), highlighting a noticeable screening effect from dipoles in the 2D case. (c), (d) Comparison of the bare 3D Coulomb potential (V_{3D}) (black solid line) and the dipole-screened 3D potential, V_{3D}^{dipole} (red solid line), in (c) momentum space and (d) real space. The dipole size remains as $d = 1.3$ nm, and the volumetric dipole density is chosen as $n_{\mathrm{dipole}}^{3D} = (10^{11})^{3/2}$ cm^{-3} for comparison with the 2D case. The dashed line and filled area represent the relative screening, $\frac{|V_{3D}^{\mathrm{screening}}-V_{3D}|}{V_{3D}}$, indicating a much weaker screening effect from dipoles in the 3D case. The inset in (c) shows a zoom-in view of the dashed region, where the dipole screening is found to be negligible.

for the bare 2D Coulomb potential, $V_{2D}(q) = \frac{e}{q(2\varepsilon_s\varepsilon_0+\alpha_{2D}q)}$ (black solid line), as well as the screened 2D Coulomb potential in the presence of 3D dipoles in a 2D plane, $V_{2D}^{3D\ \mathrm{dipole}}(q) = \frac{e}{q(2\varepsilon_s\varepsilon_0+q\alpha_{2D})-2e^2\chi_{\mathrm{dipole}}(q)[1-j_0(qd)]}$ (red solid line) and 2D dipoles in a 2D plane, $V_{2D}^{2D\ \mathrm{dipole}}(q) = \frac{e}{q(2\varepsilon_s\varepsilon_0+q\alpha_{2D})-2e^2\chi_{\mathrm{dipole}}(q)[1-J_0(qd)]}$ (blue solid line), respectively. The inset in Fig. 3(a) highlights a zoom-in view near $q = 0.2$ nm^{-1}, where noticeable reductions in both screened Coulomb potentials are observed due to the dipole screening, whether the dipole orientation is confined in the 2D plane or free to rotate in 3D space. The relative screening effect, quantified by $\frac{|V_{2D}^{\mathrm{screening}}-V_{2D}|}{V_{2D}}$, is found to be most prominent in the range $q = 0{-}0.4$ nm^{-1}, which corresponds to the selected dipole size ($d = 1.3$ nm).

Another important observation is that 2D dipoles induce stronger screening than 3D dipoles. This is because, in the 2D case, both the spatial location and orientation of the dipoles are restricted to the plane, thereby confining the screening field within the same geometry as the 2D Coulomb interaction. In contrast, 3D dipoles, which located in the 2D plane but are free to orient in three dimensions, lead to a more isotropic field distribution, reducing the effective in-plane screening. The corresponding 3D results are shown in Fig. 3(c), where a direct comparison reveals a much weaker screening effect from free dipoles in the 3D case. The inset confirms that the screened potential closely follows the unscreened one, making the screening nearly negligible in the 3D case at the corresponding dipole density $n_{\mathrm{dipole}} = (10^{11})^{\frac{3}{2}}$ cm^{-3}.

Since the analytical form of the screened Coulomb potential in real space is not readily obtainable, we evaluate it numerically, as shown in Figs. 3(b) and 3(d). In real space, the bare 2D Coulomb potential is given by $V_{2D}(\boldsymbol{\rho}) =$

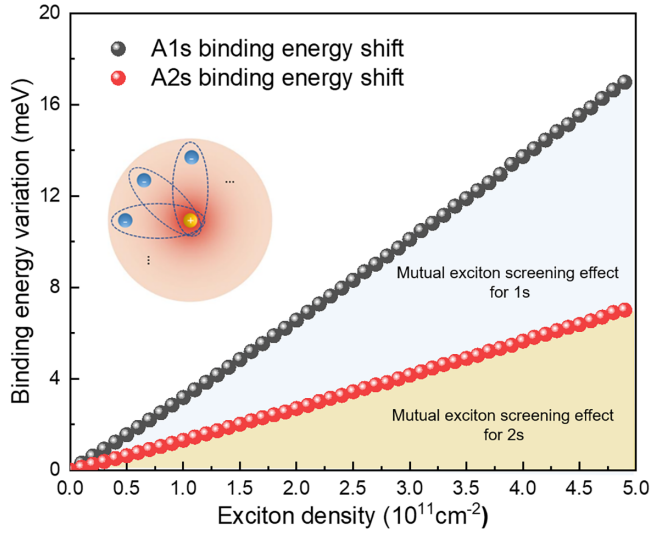

FIG. 4. Calculation of binding energy variation as a function of exciton density. Binding energy shifts of 1s state (black balls) and 2s state (red balls) excitons in monolayer TMD due to the mutual exciton screening effect as a function of exciton density.

$\frac{e}{8\varepsilon_0 r_0}[H_0(\frac{\varepsilon_s \rho}{r_0}) - Y_0(\frac{\varepsilon_s \rho}{r_0})]$; screened potentials in the presence of 2D ($V_{2D}^{2D\ \text{dipole}}(\boldsymbol{\rho})$) and 3D ($V_{2D}^{3D\ \text{dipole}}(\boldsymbol{\rho})$) dipoles show negligible deviation from the bare potential at short distances ($\rho < 0.1$ nm), but a clear suppression emerges around the $\rho \sim 0.5-5$ nm region, close to the order of magnitude of the dipole size ($d = 1.3$ nm). As ρ increases to $\sim$10 nm, the screening effect gradually decreases, as indicated by the dashed line and filled area in Fig. 3(c). In stark contrast, negligible screening is exhibited at all distances in the 3D system [Fig. 3(d)], further confirming the weak influence of free dipoles.

B. Estimation of exciton binding energy

Unlike regular dipoles, ground-state excitons do not possess permanent dipole moments owing to the s-type exciton envelope function. Nevertheless, excitons can be approximated as the composition of instantaneous dipoles with complete orientations or, in other words, the statistical average of homogeneous dipoles with different orientations, as depicted in the inset of Fig. 4. Under this simple approximation, we do not distinguish the screening effect between randomly distributed dipoles and excitons in the following text. Owing to the large binding energies of 2D materials, excitons are stable even at room temperature. Such an exciton system provides an unprecedented platform for investigating the dipole/exciton-screened Coulomb potential as a function of exciton density in the 2D case.

Recently, a report demonstrated the mutual exciton screening effect in an exciton system in monolayer $MoSe_2$. This effect was confirmed experimentally and quantified as a function of exciton density. Interestingly, the mutual exciton screening effect was found to be five times stronger than the exchange-driven exciton-exciton interaction [32]. Here, we used the derived screened Coulomb potential to account for a mutual exciton screening effect in such an exciton system. As shown in Fig. 3(a), the potential modification from dipoles mainly occurs in the range of $\sim 0-0.4$ nm^{-1}. Given that the effective Bohr radius of ground-state excitons in monolayer TMDs is approximately 1.3 nm [38], the screening effect of the exciton population can be significant. Using the dipole screening formula derived in Table I, we evaluate the change in the Coulomb potential via a perturbative term to the initial Coulomb potential under low or medium exciton densities. Specifically, the modification in the Coulomb potential between exciton-populated and zero-exciton systems, $\Delta V(\boldsymbol{q})$, can be approximated as $\Delta V(\boldsymbol{q}) \approx \frac{2e^3\chi(\boldsymbol{q})[1-J_0(qd)]}{q^2(2\varepsilon+q\alpha_{2D})^2}$. This allows us to calculate the exciton binding energy variation of the Rydberg series of excitons (1s, 2s, …) using perturbation theory, which can be expressed as

$$\langle \varphi_{ns}(\boldsymbol{r})|V(\boldsymbol{r})|\varphi_{ns}(\boldsymbol{r})\rangle = \frac{1}{(2\pi)^4}\iint \varphi_{ns}^*(\boldsymbol{k}_1)\varphi_{ns}(\boldsymbol{k}_2)\Delta V(\boldsymbol{k}_1-\boldsymbol{k}_2)d\boldsymbol{k}_1 d\boldsymbol{k}_2. \quad (16)$$

To perform this calculation, we chose the Rydberg exciton wave function from the 2D hydrogen atom model, $\psi_{1s}(\boldsymbol{k}) = 2\sqrt{2\pi}\frac{a_{B,1s}}{[1+a_{B,1s}^2k^2]^{3/2}}$ and $\psi_{2s}(\boldsymbol{k}) = 2\sqrt{6\pi}\frac{a_{B,2s}}{[1+a_{B,2s}^2k^2]^{3/2}}\frac{a_{B,2s}^2k^2-1}{a_{B,2s}^2k^2+1}$, where $a_{B,1s}$ and $a_{B,2s}$ are the Bohr radius of the ground state (1s) and the first excited state (2s). It should be noted that both 1s and 2s exciton wave functions of monolayer TMDs are mainly located in the range of $\sim 0-2$ nm^{-1}, which implies that the modified Coulomb potential due to exciton screening can effectively tune the exciton binding energy.

We performed numerical calculations using the Monte Carlo method. After a careful convergence analysis test with the sample size as shown in the Supplemental Material [33], we set the sample size to be $10^{8.5}$ and the calculated results are summarized in Fig. 4. The binding energies of 1s and 2s excitons increase almost linearly in the low and medium exciton density regimes (10^{10} cm^{-2} to 5×10^{11} cm^{-2}). However, the 2s excitons are less affected by the dipole screening, as the 2s exciton wave function is more spread out with a larger Bohr radius ($a_{B,2s} \sim 3$ nm), while the 1s exciton is more localized with a smaller Bohr radius ($a_{B,1s} \sim 1.3$ nm), making it more susceptible to the mutual screening effect. This result is consistent with previous experimental reports [32]. The calculated binding energy shift is somewhat overestimated compared to the experimental results, which may result from the difference between the actual wave functions in 2D materials and the idealized wave functions of the 2D hydrogen atom model used in our numerical calculations.

IV. CONCLUSIONS

Although estimating the exciton binding energy with elevated exciton density using the modified Coulomb potential has proven successful, the derived formula fails to accurately align the estimation of exciton binding energy as a function of carrier density. Some researchers attribute this discrepancy to the limitation of static screening [25]; we contend that its ineffectiveness stems from two more key factors. First, the exciton resonance peak comprises various contributing factors including the exciton resonance energy, electronic band gap, exciton binding energy, exciton-carrier interaction, and exciton-exciton interaction. Particularly in the

context of carrier doping, the exciton-carrier interaction is more aptly described by the Fermi-polaron picture, which arises from the collective interaction between excitons and the Fermi sea [39,40]. This complexity undermines the simplistic view of excitons solely as a two-particle (exciton) or three-particle (trion) system, thereby rendering the application of static screening approximation ineffective in this scenario. Second, it is essential to recognize that both static and dynamic screening approaches are grounded in linear response theory or perturbation theory. The validity of the screened Coulomb potential depends on whether the conditions fit in the perturbation terms and whether static or dynamic screening methodologies are employed. Consequently, the screened Coulomb potential was not applicable at high carrier densities. Nevertheless, for exciton doping at approximately 5×10^{11} cm^{-2}, the screened term can still be considered a perturbative term, as depicted in Fig. S4 in the Supplemental Material [33].

In summary, we have developed an effective model of the Coulomb potential in 2D systems that incorporates the screening effect from charge-neutral excitons and dipoles. Our methodology is based on the framework of linear response theory, which is inherently a perturbative approach. The results reveal that excitons and dipoles can significantly modify the Coulomb interaction in 2D systems due to the confinement of the excitons and dipoles in the 2D plane. The derived screened Coulomb potential provides a simple yet powerful tool to quantitatively evaluate the interaction strength in 2D materials, with implications for the design of electronic and optoelectronic devices.

ACKNOWLEDGMENTS

This work was supported by the National Key R&D Program of China (Grant No. 2020YFA0309600), the Guangdong-Hong Kong Joint Laboratory of Quantum Matter, and the Research Grants Council (RGC) of Hong Kong (Projects No. AoE/P-701/20, No. T45-406/23-R, and No. GRF 17300520). The authors thank Prof. Wang Yao, Dr. Jianju Tang, Dr. Mingyang Liu, and Dr. Yicheng Guan for their fruitful discussions. C.K. thanks Prof. Haibin Su for his support. K.X. is thankful for the support from the Max Planck Society.

DATA AVAILABILITY

The data that support the findings of this article are not publicly available. The data are available from the authors upon reasonable request.

[1] A. Chernikov, T. C. Berkelbach, H. M. Hill, A. Rigosi, Y. L. Li, O. B. Aslan, D. R. Reichman, M. S. Hybertsen, and T. F. Heinz, Exciton binding energy and nonhydrogenic Rydberg series in monolayer WS_2, Phys. Rev. Lett. **113**, 076802 (2014).

[2] P. Cudazzo, I. V. Tokatly, and A. Rubio, Dielectric screening in two-dimensional insulators: Implications for excitonic and impurity states in graphane, Phys. Rev. B **84**, 085406 (2011).

[3] B. R. Zhu, X. Chen, and X. D. Cui, Exciton binding energy of monolayer WS_2, Sci. Rep. **5**, 9218 (2015).

[4] Z. L. Ye, T. Cao, K. O'Brien, H. Y. Zhu, X. B. Yin, Y. Wang, S. G. Louie, and X. Zhang, Probing excitonic dark states in single-layer tungsten disulphide, Nature (London) **513**, 214 (2014).

[5] C. D. Zhang, A. Johnson, C. L. Hsu, L. J. Li, and C. K. Shih, Direct imaging of band profile in single layer MoS_2 on graphite: Quasiparticle energy gap, metallic edge states, and edge band bending, Nano Lett. **14**, 2443 (2014).

[6] M. M. Ugeda, A. J. Bradley, S. F. Shi, F. H. da Jornada, Y. Zhang, D. Y. Qiu, W. Ruan, S. K. Mo, Z. Hussain, Z. X. Shen *et al.*, Giant band-gap renormalization and excitonic effects in a monolayer transition metal dichalcogenide semiconductor, Nat. Mater. **13**, 1091 (2014).

[7] K. F. Mak, C. Lee, J. Hone, J. Shan, and T. F. Heinz, Atomically thin MoS_2: A new direct-gap semiconductor, Phys. Rev. Lett. **105**, 136805 (2010).

[8] K. Tran, G. Moody, F. C. Wu, X. B. Lu, J. Choi, K. Kim, A. Rai, D. A. Sanchez, J. M. Quan, A. Singh *et al.*, Evidence for moire excitons in van der Waals heterostructures, Nature (London) **567**, 71 (2019).

[9] K. L. Seyler, P. Rivera, H. Y. Yu, N. P. Wilson, E. L. Ray, D. G. Mandrus, J. Q. Yan, W. Yao, and X. D. Xu, Signatures of moire-trapped valley excitons in $MoSe_2/WSe_2$ heterobilayers, Nature (London) **567**, 66 (2019).

[10] C. Jin, E. C. Regan, A. Yan, M. Iqbal Bakti Utama, D. Wang, S. Zhao, Y. Qin, S. Yang, Z. Zheng, S. Shi *et al.*, Observation of moire excitons in WSe_2/WS_2 heterostructure superlattices, Nature (London) **567**, 76 (2019).

[11] E. Navarro-Moratalla, J. O. Island, S. Mañas-Valero, E. Pinilla-Cienfuegos, A. Castellanos-Gomez, J. Quereda, G. Rubio-Bollinger, L. Chirolli, J. A. Silva-Guillén, N. Agraït *et al.*, Enhanced superconductivity in atomically thin TaS_2, Nat. Commun. **7**, 11043 (2016).

[12] J. D. Zhou, F. C. Liu, J. H. Lin, X. W. Huang, J. Xia, B. W. Zhang, Q. S. Zeng, H. Wang, C. Zhu, L. Niu *et al.*, Large-area and high-quality 2D transition metal telluride, Adv. Mater. **29**, 1603471 (2017).

[13] Y. Xu, S. Liu, D. A. Rhodes, K. Watanabe, T. Taniguchi, J. Hone, V. Elser, K. F. Mak, and J. Shan, Correlated insulating states at fractional fillings of moire superlattices, Nature (London) **587**, 214 (2020).

[14] Y. H. Tang, L. Z. Li, T. X. Li, Y. Xu, S. Liu, K. Barmak, K. Watanabe, T. Taniguchi, A. H. MacDonald, J. Shan *et al.*, Simulation of Hubbard model physics in WSe_2/WS_2 moire superlattices, Nature (London) **579**, 353 (2020).

[15] Y. Bai, Y. Li, S. Liu, Y. Guo, J. Pack, J. Wang, C. R. Dean, J. Hone, and X. Zhu, Evidence for exciton crystals in a 2D semiconductor heterotrilayer, Nano Lett. **23**, 11621 (2023).

[16] D. Y. Qiu, F. H. da Jornada, and S. G. Louie, Screening and many-body effects in two-dimensional crystals: Monolayer MoS_2, Phys. Rev. B **93**, 235435 (2016).

[17] F. Hüser, T. Olsen, and K. S. Thygesen, How dielectric screening in two-dimensional crystals affects the convergence of excited-state calculations: Monolayer MoS_2, Phys. Rev. B **88**, 245309 (2013).
[18] K. Noori, N. L. Q. Cheng, F. Y. Xuan, and S. Y. Quek, Dielectric screening by 2D substrates, 2D Mater. **6**, 035036 (2019).
[19] L. V. Keldysh, Coulomb interaction in thin semiconductor and semimetal films, JETP Lett. **29**, 658 (1979).
[20] N. S. Rytova, Screened potential of a point charge in a thin film, Moscow Univ. Phys. Bullet. **3**, 18 (1967).
[21] N. W. Ashcroft and N. Mermin, *Solid State Physics* (Holt, Rinehart and Winston, New York, 1976).
[22] F. Stern, Polarizability of a two-dimensional electron gas, Phys. Rev. Lett. **18**, 546 (1967).
[23] T. Ando, A. B. Fowler, and F. Stern, Electronic properties of two-dimensional systems, Rev. Mod. Phys. **54**, 437 (1982).
[24] H. Haug and S. W. Koch, Semiconductor laser theory with many-body effects, Phys. Rev. A **39**, 1887 (1989).
[25] M. M. Glazov and A. Chernikov, Breakdown of the static approximation for free carrier screening of excitons in monolayer semiconductors, Phys. Status Solidi B **255**, 1800216 (2018).
[26] D. Beglov and B. Roux, An integral equation to describe the solvation of polar molecules in liquid water, J. Phys. Chem. B **101**, 7821 (1997).
[27] M. V. Fedorov and A. A. Kornyshev, Ionic liquids at electrified interfaces, Chem. Rev. **114**, 2978 (2014).
[28] D. J. Lockhart and P. S. Kim, Electrostatic screening of charge and dipole interactions with the helix backbone, Science **260**, 198 (1993).
[29] C. Neidel, J. Klei, C. H. Yang, A. Rouzée, M. J. J. Vrakking, K. Klünder, M. Miranda, C. L. Arnold, T. Fordell, A. L'Huillier *et al.*, Probing time-dependent molecular dipoles on the attosecond time scale, Phys. Rev. Lett. **111**, 033001 (2013).
[30] J. G. Gay, Screening of excitons in semiconductors, Phys. Rev. B **4**, 2567 (1971).
[31] P. D. Cunningham, A. T. Hanbicki, K. M. McCreary, and B. T. Jonker, Photoinduced band-gap renormalization and exciton binding energy reduction in WS, Acs Nano **11**, 12601 (2017).
[32] K. Xiao, T. Yan, C. Xiao, F.-R. Fan, R. Duan, Z. Liu, K. Watanabe, T. Taniguchi, S. S. Parkin, W. Yao *et al.*, Exciton–exciton interaction in monolayer $MoSe_2$ from mutual screening of Coulomb binding, Acs Nano **18**, 31869 (2024).
[33] See Supplemental Material at http://link.aps.org/supplemental/10.1103/9fgx-nq97 for Supplemental Note 1: Calculation of induced charge density associated with the dipoles based on perturbation theory in 2D and 3D case; Supplemental Note 2: Schematics of derivation process based on Linear response theory; Supplemental Note 3: 2D modified Coulomb potential from screening of 3D dipole; Supplemental Note 4: Convergence analysis test for Monte Carlo calculation of exciton binding energy; and Supplemental Note 5: Screened potential comparison for typical dipole/exciton density.
[34] F. García Flórez, L. D. Siebbeles, and H. Stoof, Effects of material thickness and surrounding dielectric medium on Coulomb interactions and two-dimensional excitons, Phys. Rev. B **102**, 125303 (2020).
[35] R. I. G. Hughes, Theoretical practice: The Bohm-Pines quartet, Persp. Sci. **14**, 457 (2006).
[36] G. D. Mahan, *Many-Particle Physics* (Springer, New York, 2000).
[37] J. H. Collet and T. Amand, Electron-hole interaction in the presence of excitons, Solid State Commun. **52**, 53 (1984).
[38] M. Goryca, J. Li, A. V. Stier, T. Taniguchi, K. Watanabe, E. Courtade, S. Shree, C. Robert, B. Urbaszek, and X. Marie, Revealing exciton masses and dielectric properties of monolayer semiconductors with high magnetic fields, Nat. Commun. **10**, 4172 (2019).
[39] E. F. Liu, J. van Baren, Z. G. Lu, T. Taniguchi, K. Watanabe, D. Smirnov, Y. C. Chang, and C. H. Lui, Exciton-polaron Rydberg states in monolayer $MoSe_2$ and WSe_2, Nat. Commun. **12**, 6131 (2021).
[40] K. Xiao, T. F. Yan, Q. Y. Liu, S. Y. Yang, C. M. Kan, R. H. Duan, Z. Liu, and X. D. Cui, Many-body effect on optical properties of monolayer molybdenum diselenide, J. Phys. Chem. Lett. **12**, 2555 (2021).